

## Synthesis and Photocatalytic Activity of TiO<sub>2</sub> on Phenol Degradation

Muhamad D. Permana<sup>1</sup>, Atiek R. Noviyanti<sup>1</sup>, Putri R. Lestari<sup>2</sup>, Nobuhiro Kumada<sup>2</sup>, Diana R. Eddy<sup>1,\*</sup>,  
Iman Rahayu<sup>1</sup>

<sup>1</sup>*Dept. of Chemistry, Faculty Mathematics and Natural Sciences, Universitas Padjadjaran  
Sumedang, West Java-45363, Indonesia*

<sup>2</sup>*Center for Crystal Science and Technology, University of Yamanashi  
Kofu, Yamanashi 400-8511, Japan*

\*Corresponding Author: [diana.rahmawati@unpad.ac.id](mailto:diana.rahmawati@unpad.ac.id)

### Abstract

Photocatalysis is a process of accelerating reactions that are assisted by energy from light irradiation. Titanium dioxide (TiO<sub>2</sub>) is one of the most widely developed photocatalysis materials, and is used because of its high catalytic activity, stability and very affordable. The most commonly used precursors of TiO<sub>2</sub> are titanium butoxide (TBOT) and titanium tetraisopropoxide (TTIP). These variations in precursor can lead to phase difference in the formation of TiO<sub>2</sub> crystals, which further improves its nature in the activity of photocatalysis. In this study, the sol-gel method was used to synthesize titanium dioxide nanoparticles from variations of TBOT and TTIP. Furthermore, the structure, crystallite size and band gap of TiO<sub>2</sub> were determined by X-ray diffraction (XRD) and UV-vis reflectance spectroscopy (DRS). Subsequently, TiO<sub>2</sub> photocatalytic activity was evaluated in phenol photodegradation as a contaminant model with UV irradiation. The results showed the structure synthesized from TBOT had a higher amount of anatase, higher crystallinity, smaller crystallite size, larger band gap, and better photocatalytic activity than those from TTIP. Furthermore, it was shown that TiO<sub>2</sub> from TBOT had an efficiency of 147% greater than TiO<sub>2</sub> P25 Degussa, while TiO<sub>2</sub> from TTIP had 66% efficiency compared to TiO<sub>2</sub> P25.

**Keywords:** Phenol; photocatalyst; TiO<sub>2</sub>; TBOT; TTIP

### 1. Introduction

Phenols are toxic chemical compounds and they are slowly degraded in the environment to form different aromatic intermediates. In fact, most of them cause environmental hazards (Peiró *et al.*, 2001). Nevertheless, this compound and its intermediates can be reduced by various methods, which include photocatalysis (Lestari *et al.*, 2021), ozonation (Shahamat *et al.*, 2014; Wei *et al.*, 2020), adsorption (Miao *et al.*, 2013; Zhang *et al.*, 2016; Dehmani *et al.*, 2020), biological (Pradeep *et al.*, 2015), and Fenton

methods (Gümüş & Akbal, 2016; Yazdanbakhsh *et al.*, 2020). Although the most suitable and widely used method is photocatalysis due to its advantages of efficient industrial waste degradation (Ameta & Ameta, 2016), affordability, and environmentally friendly (Chong *et al.*, 2010).

Titanium dioxide (TiO<sub>2</sub>) is an effective photocatalyst and it is applied in various fields such as environmental and energy, including self-cleaning surfaces (Tavares *et al.*, 2014; Banerjee *et al.*, 2015), air and water purification systems (Turkay & Kumbur, 2019; Mamaghani

*et al.*, 2020), sterilization (Junkar *et al.*, 2016), and photoelectrochemical conversion (Wang *et al.*, 2011; Nakata & Fujishima, 2012). The main advantages of this compound include high chemical stability under acidic and basic conditions, non-toxic, affordability, and is an environmentally safe oxidizer, making it potential for many photocatalytic applications (Eddy *et al.*, 2018; Alkhayatt *et al.*, 2021).

The TiO<sub>2</sub> is divided into 3 main phases namely anatase, rutile, and brookite (Haggerty *et al.*, 2017). Generally, anatase has the best photocatalytic ability compared to others because it shows a deeper excited charge carrier in large part leading to a higher surface reaction (Luttrell *et al.*, 2014). Heterophase of TiO<sub>2</sub> can effectively stimulate electron transfer from one phase to another which helps to increase its photocatalytic performance (Hu *et al.*, 2018; Ding *et al.*, 2020). For instance, the well-known TiO<sub>2</sub> P25 Degussa which consists of ~20% rutile and ~80% anatase, is an exceptionally good photocatalyst (Berger *et al.*, 2005).

Most of this compound was synthesized using organometallic precursors such as titanium butoxide (TBOT) (Gan *et al.*, 2018; Wang *et al.*, 2018; Lenzion-Bieluń *et al.*, 2020) and titanium tetraisopropoxide (TTIP) (Cenovar *et al.*, 2012; Paunović *et al.*, 2015). The inorganic alkoxide precursor is preferred because of its ability to hydrolyze easily to the oxide phase due to its exposure to water (Syoufian *et al.*, 2007).

Behnajady *et al.* (2011) investigated the conditions of TiO<sub>2</sub> synthesis using TBOT and TTIP for photocatalysis on the removal of C.I. Acid Red27 (AR27). Niu *et al.* (2014) also reported the synthesis of nanoparticles of this compound by microwave radiation method under difference precursor between TiCl<sub>4</sub>, Ti(SO<sub>4</sub>)<sub>2</sub>, and TBOT for photocatalytic degradation of methylene blue (MB).

Cenovar *et al.* (2012) reported that they have successfully synthesized TiO<sub>2</sub> using the sol-gel method from TTIP. The results showed anatase had a stable crystal structure within the temperature range of 250 - 650°C. Zhao *et al.* (2009) reported a tested and proven effective method to synthesize brookite TiO<sub>2</sub> which is using hydrothermal methods or reflux conditions from the TBOT precursor. The results showed

crystal structure of pure anatase, pure brookite, and brookite/anatase mixtures were formed.

However, there has been no report showing comparison in the effect of TBOT and TTIP precursors on TiO<sub>2</sub> crystal properties and their activity on phenol degradation. In this study, the compound was synthesized by sol-gel method from organometallic TBOT and TTIP. The effect of these parameters was further investigated on the crystal phase, size, lattice parameters, band gap energy, and its photocatalytic activity in phenol degradation.

## 2. Materials and Methods

### 2.1 Materials

The materials used in this study were ethanol (C<sub>2</sub>H<sub>5</sub>OH, 99%, Merck), phenol (C<sub>6</sub>H<sub>5</sub>OH, 99%, Merck), TiO<sub>2</sub> nanoparticles (P25 Degussa, 20% rutile and 80% anatase, Merck), titanium butoxide (TBOT, Ti(OC<sub>4</sub>H<sub>9</sub>)<sub>4</sub>, 99%, Sigma Aldrich), and titanium tetraisopropoxide (TTIP, Ti(OC<sub>3</sub>H<sub>7</sub>)<sub>4</sub>, 99%, Sigma Aldrich). All ingredients were used without treatment.

### 2.2 Synthesis of TiO<sub>2</sub>

Ethanol 95 mL and 0.48 mL of distilled water were mixed together and stirred for 30 mins, then a TiO<sub>2</sub> precursor (1.5 mL TBOT or 2.0 mL TTIP) in 18 mL ethanol was injected into the mixture at a rate of 0.5 mL/min using a syringe pump. After injection, the temperature was raised to 85°C under reflux at a stirring speed of 900 rpm for 100 mins. Furthermore, the precipitate was isolated by centrifugation, washed with distilled water and ethanol, dried in vacuum, and calcined at 800°C for 2 hours in the air to obtain TiO<sub>2</sub> TBOT (representing TiO<sub>2</sub> synthesized from the precursor TBOT) and TiO<sub>2</sub> TTIP (representing TiO<sub>2</sub> synthesized from the precursor TTIP).

### 2.3 Characterization of TiO<sub>2</sub>

X-ray diffraction (XRD) patterns were obtained on a Rigaku/MiniFlex 600, and then measured at room temperature with Cu K $\alpha$  radiation ( $\lambda = 1.5418 \text{ \AA}$ ). The scan ranged from 20 to 80 (2 $\theta$ ). Also, the crystallite size was determined by using the Debye-Scherrer equation (Eddy *et al.* 2020):

$$B = K\lambda / D \cos \theta \quad (1)$$

Where D is the crystal size, K is the Scherrer constant (0.9),  $\lambda$  is the wavelength of the X-ray radiation, B is the value of the peak FWHM (full width at half maximum), and  $\theta$  is the angle of diffraction.

Crystallinity was calculated by comparing the crystalline peak ( $I_c$ ) with the total (crystalline peak ( $I_c$ ) and amorphous peak ( $I_a$ )).

$$\text{Crystallinity (\%)} = I_c / (I_c + I_a) \times 100\% \quad (2)$$

A Jasco V-550 spectroscopy was used to record the UV-visible (UV-vis) spectra, and the analysis range was from 200 to 800 nm. The optical band gap energy ( $E_g$ ) was obtained using the Tauc equation:

$$(\alpha h\nu)^{1/n} = A(h\nu - E_g) \quad (3)$$

where  $\alpha$  is the absorption coefficient,  $h\nu$  is photon energy, and A is the proportionality constant. Furthermore, the transition property is represented by n, where n = 2 for the indirect band gap allowed (Chowdhury *et al.* 2019).

#### 2.4 Photocatalytic Analysis

Photocatalytic degradation was carried out with 50 mL of a 20 mg/L phenol solution with 15 mg catalyst, within a period of 60 mins under dark adsorption (no irradiation source). Subsequently, the mixture was stirred at 300 rpm for 2 hours under light irradiation (300 W Xe lamp, UV ray with wavelength <390 nm, PE300BUV) at a distance of 150 mm above the surface of the solution. Furthermore, the time was tested to determine the remaining phenol concentration using reverse-phase high-performance liquid chromatography (HPLC, Jasco Co-2065Plus), with UV detector (Jasco UV-2075Plus), C-18 column or Octadecyl Silica (ODS) as the stationary phase and a mixture of distilled water and methanol as the mobile phase. The HPLC used methanol:water (1:1) as eluent, with a column temperature of 40°C and a column flow rate of 1.00 mL/min (Lestari *et al.*, 2020).

The equation below was used to calculate the percentage of phenol adsorption and degradation:

$$\% \text{ Removing} = (C_i - C_t) / C_i \times 100\% \quad (4)$$

Where  $C_i$  is the initial phenol concentration and  $C_t$  is phenol concentration at time t.

The kinetics of photocatalysis were calculated using first and second-order models. The first-order kinetics were calculated (Eddy *et al.*, 2020):

$$\ln(C_i/C_t) = -k_1 t + b \quad (5)$$

Where,  $C_i$  denotes the initial phenol concentration ( $\text{mg.L}^{-1}$ ),  $C_t$  is the phenol concentration ( $\text{mg.L}^{-1}$ ) in solution at t mins, b denotes the constant, and  $k_1$  ( $\text{min}^{-1}$ ) is the first-order rate constant. Then a second-order kinetics model was calculated based on the rate obtained from square of the number of sites on the catalyst surface (Turki *et al.*, 2015). The equation after integration is obtained as:

$$1/C_t - 1/C_i = -k_2 t + b \quad (6)$$

Where,  $k_2$  denotes the second-order rate constant ( $\text{L.mol}^{-1}.\text{min}^{-1}$ ).

### 3. Result and Discussion

#### 3.1 Characterization of Photocatalyst

##### 3.1.1 X-ray diffraction Analysis

The results of X-ray diffraction (XRD) analysis are shown in Figure 1. The XRD patterns of P25,  $\text{TiO}_2$  TBOT, and  $\text{TiO}_2$  TTIP showed similarity with the Inorganic Crystal Structure Database (ICSD) 98-017-2914 for anatase (tetragonal, space group  $I4_1/amd$ ) and ICSD 98-016-7961 for rutile (tetragonal, space group  $P4_2/mmm$ ). The highest peak of P25 was attained at  $2\theta = 25.27^\circ$ , while the highest peak of  $\text{TiO}_2$  TBOT was observed at  $2\theta = 25.25^\circ$ , and the highest peak of  $\text{TiO}_2$  TTIP was at  $2\theta = 27.38^\circ$ . Also, P25 and  $\text{TiO}_2$  TBOT had the highest peaks in relation to the anatase at  $2\theta = 25.30^\circ$ , while  $\text{TiO}_2$  TTIP had the highest peaks in relation to rutile at  $2\theta = 27.43^\circ$ .

$\text{TiO}_2$  P25 Degussa crystals showed peak pattern at  $2\theta = 25.3^\circ$  (011),  $37.8^\circ$  (004),  $48.0^\circ$  (020),  $53.9^\circ$  (015),  $55.0^\circ$  (121),  $62.7^\circ$  (024),  $68.8^\circ$  (116),  $70.3^\circ$  (220), and  $75.1^\circ$  (125) in the crystalline plane of anatase. In addition, the

peaks at  $27.4^\circ$  (110) and  $36.1^\circ$  (011) were obtained from the rutile phase plane. For  $\text{TiO}_2$  TBOT, there were additional peaks at  $41.23^\circ$  (111) and  $44.04^\circ$  (120) which were considered to be from the rutile phase. This was also observed in  $\text{TiO}_2$  TTIP at  $41.23^\circ$  (111),  $44.04^\circ$  (120),  $54.31^\circ$  (121),  $56.62^\circ$  (220), and  $68.99^\circ$  (031), and is considered to have been derived from the rutile phase.

**Table 1.** Percentage of anatase and rutile phase in photocatalysts.

Photocatalysts	Phase (%)	
	Anatase	Rutile
$\text{TiO}_2$ P25	85.7	14.3
$\text{TiO}_2$ TBOT	33.2	66.8
$\text{TiO}_2$ TTIP	0.9	99.1

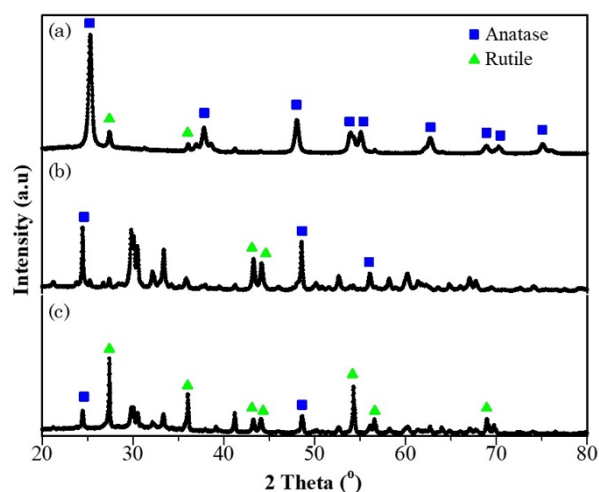


**Fig. 1.** XRD pattern of photocatalyst (a) P25, (b)  $\text{TiO}_2$  TBOT, and (c)  $\text{TiO}_2$  TTIP.

A Rietveld refinement of the  $\text{TiO}_2$  sample was performed from the XRD pattern. The percentage of  $\text{TiO}_2$  phase is shown in Table 1. At

the same calcination temperature ( $800^\circ\text{C}$ ),  $\text{TiO}_2$  TBOT had a higher anatase percentage (33.2%) than  $\text{TiO}_2$  TTIP (0.9%). This showed that different precursors require different energy to form its crystal lattice. These results can be compared to Behnajady *et al.* (2011) which stated that  $\text{TiO}_2$  synthesized through the TBOT precursor produced a higher percentage of anatase than  $\text{TiO}_2$  from TTIP.

**Table 2.** The crystallinity and crystallite size of photocatalysts.

Photocatalysts	Crystallinity (%)	Crystallite size (nm)	
		Anatase	Rutile
$\text{TiO}_2$ P25	46.01	32.84	22.59
$\text{TiO}_2$ TBOT	75.67	75.28	73.37
$\text{TiO}_2$ TTIP	60.57	81.44	52.23

Table 2 shows the crystallinity and crystallite size of photocatalysts. It shows that the synthesis from TBOT and TTIP precursors have a higher crystallinity than  $\text{TiO}_2$  P25 Degussa. Meanwhile, high crystallinity is required in photocatalysis because of its ability to prevent the possibility of electron-hole recombination, in order to increase photocatalytic activity (Zheng *et al.* 2018). However, those from TBOT have higher crystallinity than those from TTIP which can support photocatalysis.

The crystallite size of the synthesized  $\text{TiO}_2$  showed a larger size than Degussa  $\text{TiO}_2$  P25 in anatase and rutile. This result was possible due to the sol-gel method which increased the crystallite size. However, those from the TBOT showed smaller size in anatase (75.28 nm) than those from the TTIP (81.44 nm). Also, in the rutile phase,  $\text{TiO}_2$  from TBOT showed a larger size (73.37 nm) than  $\text{TiO}_2$  from TTIP (52.23 nm).

**Table 3.** The crystal lattice parameters of photocatalysts.

Photocatalyst	Anatase			Rutile		
	$a=b$ (Å)	$c$ (Å)	$V(\text{Å}^3)$	$a=b$ (Å)	$c$ (Å)	$V(\text{Å}^3)$
ICSD 98-017-2914	3.78	9.51	136.27	-	-	-
ICSD 98-016-7961	-	-	-	4.59	2.96	62.47
$\text{TiO}_2$ P25	3.78	9.50	136.11	4.59	2.96	62.32
$\text{TiO}_2$ TBOT	3.78	9.50	135.89	4.59	2.96	62.38
$\text{TiO}_2$ TTIP	3.73	9.37	130.36	4.59	2.96	62.42

Table 3 shows the lattice parameters of TiO<sub>2</sub>, and it is seen that the synthesized substance has anatase crystals with a smaller lattice than TiO<sub>2</sub> P25 Degussa. Furthermore, those from the TTIP have smaller lattice than those from the TBOT with a crystal lattice volume of 135.8914 Å<sup>3</sup> for TiO<sub>2</sub> TBOT and 130.3639 Å<sup>3</sup> for TiO<sub>2</sub> TTIP. Whereas in rutile crystals, the synthesized substance showed a larger lattice than TiO<sub>2</sub> P25 Degussa. A comparison of the precursor synthesis was also done, and it was observed that those of TTIP have larger lattice with a volume of 62.4220 Å<sup>3</sup> compared to TBOT, with a crystal lattice volume of 62.3819 Å<sup>3</sup>. This shows that synthesizing this compound by sol-gel method can decrease the anatase crystal lattice and increase rutile. This effect occurs more in synthesis from TTIP precursors than those from TBOT.

**Table 4.** The band gap of photocatalysts.

Photocatalysts	Wavelength (nm)	Band gap (eV)
TiO <sub>2</sub> P25	411.9	3.01
TiO <sub>2</sub> TBOT	414.7	2.99
TiO <sub>2</sub> TTIP	439.7	2.82

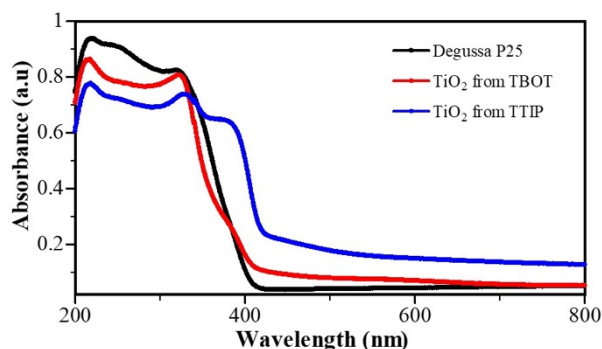


**Fig. 2.** Photocatalysts absorption in range 200-800 nm.

### 3.1.2 UV-vis Spectroscopy Analysis

The UV-vis absorption spectrum is shown in Figure 2. TiO<sub>2</sub> P25 Degussa has clear ultraviolet light absorption characteristics and does not absorb visible light. However, those synthesized from the TTIP has absorption characteristics that extends from 350 nm to 413 nm, and attain its maximum absorption at 385 nm. The red shift of TiO<sub>2</sub> uptake from TBOT and TiO<sub>2</sub> from TTIP compared to TiO<sub>2</sub> P25 Degussa showed there

was a decrease in the band gap for the synthesized TiO<sub>2</sub>.

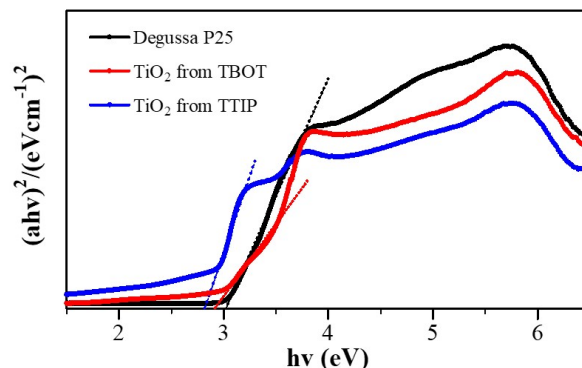


**Fig. 3.** The band gap of a photocatalysts using Tauc equation.

Band gap energy is calculated by plotting  $(ahv)^2$  vs  $h\nu$  (Figure 3). The values for P25, TiO<sub>2</sub> from TBOT, and TiO<sub>2</sub> from TTIP are shown in Table 4. Therefore, it is seen that the synthesized TiO<sub>2</sub> causes a slight decrease in band gap than P25 Degussa. This is due to the formation of rutile phase, which is more dominant than anatase, where the standard anatase has a band gap of 3.2 eV and rutile has 3.0 eV (Luttrell *et al.* 2014). In addition, TiO<sub>2</sub> from TTIP has a smaller band gap value (2.82 eV) because it has a more rutile phase than TiO<sub>2</sub> from TBOT (2.99 eV). The values determined in this work are all smaller than those reported in other literatures.

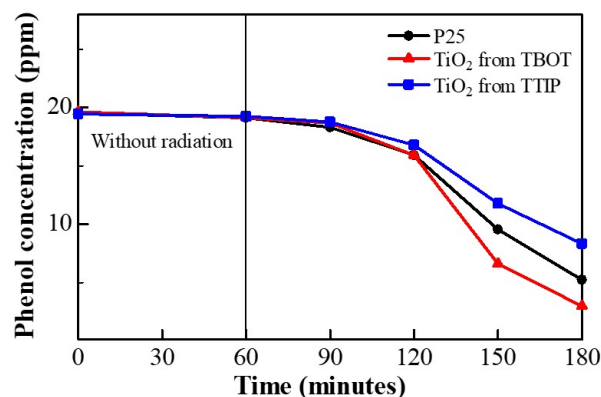


**Fig. 4.** Photocatalytic activity of catalyst on phenol. The experiment was conducted using 50 mL phenol solution 20 mg/L and 15 mg catalyst with 180 min treatment.

Also, variations in the band gap value can be influenced by differences in the crystal lattice parameters. This causes changes of electron density in the crystal (Barajas-Aguilar *et al.*, 2018), therefore, the band gap value can be changed.

**Table 5.** The percentage efficiency of phenol adsorption and degradation.

Photocatalysts	Phenol adsorption (%)	Phenol degradation (%)
TiO <sub>2</sub> P25	2.04	71.15
TiO <sub>2</sub> TBOT	2.46	82.38
TiO <sub>2</sub> TTIP	1.04	56.14

### 3.2 Photocatalytic Activity

Experimental results of the photocatalytic degradation of phenol are shown in Figure 4. The activity of photocatalysts exposed to UV rays has better percentage degradation when compared to those not exposed. This showed photons from UV light have a positive effect on photocatalyst performance in phenol oxidation.

Table 5 shows the percentage adsorption and degradation of phenol by photocatalysts. It can be seen that TiO<sub>2</sub> from the TBOT had the largest percentage of adsorption (2.46%) which correlates with the largest percentage of degradation (82.38%). In contrast, those from TTIP have the lowest percentage of adsorption (1.04%) and degradation (56.14%) compared to TBOT and P25 Degussa after 2 hours of UV irradiation. This is because TiO<sub>2</sub> from TBOT has the highest crystallinity which reduces the occurrence of recombination (Zheng *et al.* 2018), while the smaller crystallite anatase size increases the photocatalytic ability. Furthermore, it had a greater percentage of anatase (33.2%) than the other. The presence of this anatase-rutile heterophase enhances the formation of an electron synergistic effect, which effectively stimulates the transfer of electrons from one phase to another (Hu *et al.*, 2018; Ding *et al.*, 2020). Although its amount of anatase was too low (0.9%), therefore, this effect might not occur.

Table 6 shows the reaction of kinetic rate constant data based on the pseudo first and second-order models. It is seen that the pseudo first-order model gives a better R-value than the

second. This implies that the photocatalytic reaction of phenol degradation fits it. Meanwhile, the highest  $k$  value is found in TiO<sub>2</sub> from the TBOT precursor in both models, namely with  $k_1$  of 0.0159 min<sup>-1</sup> in the first-order model and  $k_2$  of 0.0017 L.mol<sup>-1</sup>.min<sup>-1</sup> in the second. The  $k_1$  value in the first is followed by Degussa TiO<sub>2</sub> P25 (0.0108 min<sup>-1</sup>) and TiO<sub>2</sub> TTIP (0.0071 min<sup>-1</sup>).

**Table 6.** The kinetic study of photocatalysts.

Sample	Pseudo first-order		Pseudo second-order	
	$k_1$	R <sup>2</sup>	$k_2$	R <sup>2</sup>
TiO <sub>2</sub> P25	0.0108	0.8663	0.0008	0.6651
TiO <sub>2</sub> TBOT	0.0159	0.8505	0.0017	0.6315
TiO <sub>2</sub> TTIP	0.0071	0.8859	0.0004	0.7243

The results showed the efficiency of phenol removal with TiO<sub>2</sub> from TBOT was 147% greater than TiO<sub>2</sub> P25 Degussa for the first-order model, while TiO<sub>2</sub> from TTIP had 66% efficiency compared to TiO<sub>2</sub> P25 Degussa.

## 4. Conclusions

In this study, the sol-gel method was used to synthesize titanium dioxide from variations of the TBOT and TTIP precursors and tested for photocatalytic activity on phenol. Results show that TBOT makes TiO<sub>2</sub> dominant with the anatase phase. Also, TiO<sub>2</sub> synthesized from TBOT has high crystallinity, small crystallite size, and higher band gap than TiO<sub>2</sub> from TTIP. In addition, TiO<sub>2</sub> synthesized from TBOT precursor has a higher photocatalytic activity than TiO<sub>2</sub> P25 Degussa with greater efficiency of 147%, while that from TTIP has an efficiency of 66%.

## ACKNOWLEDGEMENT

The authors would like to thank the Universitas Padjadjaran for facilities.

## References

- Alkhayatt, A.H.O., Hussain, S.A. & Muhammad, S.K. (2021) Hydrothermally growth of TiO<sub>2</sub> Nanorods, characterization and annealing temperature effect. *Kuwait Journal of Science*, **48**(3).
- Ameta, R. & Ameta, S.C. (2016) *Photocatalysis: principles and applications*. CRC Press, Boca Raton.
- Banerjee, S., Dionysiou, D.D. & Pillai, S.C. (2015) Self-cleaning applications of TiO<sub>2</sub> by photo-induced hydrophilicity and photocatalysis. *Applied Catalysis B: Environmental*, **176**: 396-428.
- Barajas-Aguilar, A.H., Irwin, J.C., Garay-Tapia, A.M., Schwarz, T., Delgado, F.P., Brodersen, P.M., Prinja, R., Kherani, N. & Sandoval, S.J.J. (2018) Crystalline structure, electronic and lattice-dynamics properties of NbTe<sub>2</sub>. *Scientific Reports*, **8**(1): 1-14.
- Behnajady, M.A., Eskandarloo, H., Modirshahla, N. & Shokri, M. (2011) Investigation of the effect of sol-gel synthesis variables on structural and photocatalytic properties of TiO<sub>2</sub> nanoparticles. *Desalination*, **278**(1-3): 10-17
- Berger, T., Sterrer, M., Diwald, O., Knözinger, E., Panayotov, D., Thompson, T.L. & Yates, J.T. (2005) Light-induced charge separation in anatase TiO<sub>2</sub> particles. *The Journal of Physical Chemistry B*, **109**(13): 6061-6068.
- Cenovar, A., Paunovic, P., Grozdanov, A., Makreski, P. & Fidancevska, E. (2012) Preparation of nano-crystalline TiO<sub>2</sub> by Sol-gel method using titanium tetraisopropoxide (TTIP) as a precursor. *Advances in Natural Science: Theory & Applications*, **1**(2): 133-142.
- Chong, M.N., Jin, B., Chow, C.W. & Saint, C. (2010) Recent developments in photocatalytic water treatment technology: a review. *Water research*, **44**(10): 2997-3027.
- Chowdhury, I.H., Roy, M., Kundu, S. & Naskar, M.K. (2019) TiO<sub>2</sub> hollow microspheres impregnated with biogenic gold nanoparticles for the efficient visible light-induced photodegradation of phenol. *Journal of Physics and Chemistry of Solids*, **129**: 329-339.
- Dehmani, Y., Sellaoui, L., Alghamdi, Y., Lainé, J., Badawi, M., Amhoud, A., Bonilla-Petriciolet, A., Lamhasni, T. & Abouarnadasse, S. (2020) Kinetic, thermodynamic and mechanism study of the adsorption of phenol on Moroccan clay. *Journal of Molecular Liquids*, **312**: 113383.
- Ding, L., Yang, S., Liang, Z., Qian, X., Chen, X., Cui, H. & Tian, J. (2020) TiO<sub>2</sub> nanobelts with anatase/rutile heterophase junctions for highly efficient photocatalytic overall water splitting. *Journal of Colloid and Interface Science*, **567**: 181-189.
- Eddy, D.R., Anggraeni, A., Fauzia, R.P., Rahayu, I., Mutalib, A., Firdaus, M.L. & Bahti, H.H. (2018) Gadolinium-Mesoporous Silica as a Potential Magnetic Resonance Imaging Contrast Agents. *Oriental Journal of Chemistry*, **34**(5): 2603.
- Eddy, D.R., Ishmah, S.N., Permana, M.D. & Firdaus, M.L. (2020) Synthesis of Titanium Dioxide/Silicon Dioxide from Beach Sand as Photocatalyst for Cr and Pb Remediation. *Catalysts*, **10**(11): 1248.
- Gan, Y., Wei, Y., Xiong, J. & Cheng, G. (2018) Impact of post-processing modes of precursor on adsorption and photocatalytic capability of mesoporous TiO<sub>2</sub> nanocrystallite aggregates towards ciprofloxacin removal. *Chemical Engineering Journal*, **349**: 1-16.
- Gümüş, D. & Akbal, F. (2016) Comparison of Fenton and electro-Fenton processes for oxidation of phenol. *Process Safety and Environmental Protection*, **103**: 252-258.
- Haggerty, J.E., Schelhas, L.T., Kitchaev, D.A., Mangum, J.S., Garten, L.M., Sun, W., Stone, K.H., Perkins, J.D., Toney, M.F., Ceder, G. & Ginley, D.S. (2017) High-fraction brookite films from amorphous precursors. *Scientific Reports*, **7**(1): 1-11.
- Hu, J., Zhang, S., Cao, Y., Wang, H., Yu, H. & Peng, F. (2018) Novel highly active anatase/rutile TiO<sub>2</sub> photocatalyst with hydrogenated heterophase interface structures

for photoelectrochemical water splitting into hydrogen. *ACS Sustainable Chemistry & Engineering*, **6**(8): 10823-10832.

**Junkar, I., Kulkarni, M., Drašler, B., Rugelj, N., Mazare, A., Flašker, A., Drobne, D., Humpolčiček, P., Resnik, M., Schmuki, P. & Mozetič, M. (2016)** Influence of various sterilization procedures on TiO<sub>2</sub> nanotubes used for biomedical devices. *Bioelektrochemie*, **109**: 79-86.

**Lenzion-Bieluń, Z., Wojciechowska, A., Grzechulska-Damszel, J., Narkiewicz, U., Śniadecki, Z. & Idzikowski, B. (2020)** Effective processes of phenol degradation on Fe<sub>3</sub>O<sub>4</sub>-TiO<sub>2</sub> nanostructured magnetic photocatalyst. *Journal of Physics and Chemistry of Solids*, **136**: 109178.

**Lestari, P.R., Takei, T. & Kumada, N. (2021)** Novel ZnTi/C<sub>3</sub>N<sub>4</sub>/Ag LDH heterojunction composite for efficient photocatalytic phenol degradation. *Journal of Solid State Chemistry*, **294**: 121858.

**Lestari, P.R., Takei, T., Yanagida, S. & Kumada, N. (2020)** Facile and controllable synthesis of Zn-Al layered double hydroxide/silver hybrid by exfoliation process and its plasmonic photocatalytic activity of phenol degradation. *Materials Chemistry and Physics*, **250**: 122988.

**Luttrell, T., Halpegamage, S., Tao, J., Kramer, A., Sutter, E. & Batzill, M. (2014)** Why is anatase a better photocatalyst than rutile? -Model studies on epitaxial TiO<sub>2</sub> films. *Scientific Reports*, **4**(1): 1-8.

**Mamaghani, A.H., Haghghat, F. & Lee, C.S. (2020)** Role of titanium dioxide (TiO<sub>2</sub>) structural design/morphology in photocatalytic air purification. *Applied Catalysis B: Environmental*, **269**: 118735.

**Miao, Q., Tang, Y., Xu, J., Liu, X., Xiao, L. & Chen, Q. (2013)** Activated carbon prepared from soybean straw for phenol adsorption. *Journal of the Taiwan Institute of Chemical Engineers*, **44**(3): 458-465.

**Nakata, K. & Fujishima, A. (2012)** TiO<sub>2</sub> photocatalysis: Design and applications. *Journal*

of Photochemistry and Photobiology C: Photochemistry Reviews, **13**(3): 169-189.

**Niu, J., Yao, B., Peng, C., Zhang, W. & Chen, Y. (2014)** Rapid microwave hydrothermal methods synthesis of TiO<sub>2</sub> photocatalysts using different sources of materials. *Integrated Ferroelectrics*, **152**(1): 163-173.

**Paunović, P., Grozdanov, A., Češnovar, A., Makreski, P., Gentile, G., Ranguelov, B. & Fidančevska, E. (2015)** Characterization of nanoscaled TiO<sub>2</sub> produced by simplified sol-gel method using organometallic precursor. *Journal of Engineering Materials and Technology*, **137**(2).

**Peiro, A.M., Ayllón, J.A., Peral, J. & Doménech, X. (2001)** TiO<sub>2</sub>-photocatalyzed degradation of phenol and ortho-substituted phenolic compounds. *Applied Catalysis B: Environmental*, **30**(3-4): 359-373.

**Pradeep, N.V., Anupama, S., Navya, K., Shalini, H.N., Idris, M. & Hampannavar, U.S. (2015)** Biological removal of phenol from wastewaters: a mini review. *Applied Water Science*, **5**(2): 105-112.

**Shahamat, Y.D., Farzadkia, M., Nasser, S., Mahvi, A.H., Gholami, M. & Esrafil, A. (2014)** Magnetic heterogeneous catalytic ozonation: a new removal method for phenol in industrial wastewater. *Journal of Environmental Health Science and Engineering*, **12**(1): 1-12.

**Syoufian, A., Inoue, Y., Yada, M. & Nakashima, K. (2007)** Preparation of submicrometer-sized titania hollow spheres by templating sulfonated polystyrene latex particles. *Materials Letters*, **61**(7): 1572-1575.

**Tavares, M.T.S., Santos, A.S.F., Santos, I.M.G., Silva, M.R.S., Bomio, M.R.D., Longo, E., Paskocimas, C.A. & Motta, F.V. (2014)** TiO<sub>2</sub>/PDMS nanocomposites for use on self-cleaning surfaces. *Surface and Coatings Technology*, **239**: 16-19.

**Turkay, G.K. & Kumbur, H. (2019)** Investigation of amoxicillin removal from aqueous solution by Fenton and photocatalytic oxidation processes. *Kuwait Journal of Science*, **46**(2).

**Turki, A., Guillard, C., Dappozze, F., Ksibi, Z., Berhault, G. & Kochkar, H. (2015)** Phenol photocatalytic degradation over anisotropic TiO<sub>2</sub> nanomaterials: Kinetic study, adsorption isotherms and formal mechanisms. *Applied Catalysis B: Environmental*, **163**: 404-414.

**Wang, G., Wang, H., Ling, Y., Tang, Y., Yang, X., Fitzmorris, R.C., Wang, C., Zhang, J.Z. & Li, Y. (2011)** Hydrogen-treated TiO<sub>2</sub> nanowire arrays for photoelectrochemical water splitting. *Nano letters*, **11**(7): 3026-3033.

**Wang, X., Bai, L., Liu, H., Yu, X., Yin, Y. & Gao, C. (2018)** A Unique Disintegration–Reassembly Route to Mesoporous Titania Nanocrystalline Hollow Spheres with Enhanced Photocatalytic Activity. *Advanced Functional Materials*, **28**(2): 1704208.

**Wei, X., Shao, S., Ding, X., Jiao, W. & Liu, Y. (2020)** Degradation of phenol with heterogeneous catalytic ozonation enhanced by high gravity technology. *Journal of Cleaner Production*, **248**: 119179.

**Yazdanbakhsh, A., Aliyari, A., Sheikhmohammadi, A. & Aghayani, E. (2020)** Application of the enhanced sono-photo-Fenton-like process in the presence of persulfate for the simultaneous removal of chromium and phenol from the aqueous solution. *Journal of Water Process Engineering*, **34**: 101080.

**Zhang, D., Huo, P. & Liu, W. (2016)** Behavior of phenol adsorption on thermal modified activated carbon. *Chinese Journal of Chemical Engineering*, **24**(4): 446-452.

**Zhao, B., Chen, F., Huang, Q. & Zhang, J. (2009)** Brookite TiO<sub>2</sub> nanoflowers. *Chemical Communications*, (34): 5115-5117.

**Zheng, H., Svengren, H., Huang, Z., Yang, Z., Zou, X. & Johnsson, M. (2018)** Hollow titania spheres loaded with noble metal nanoparticles for photocatalytic water oxidation. *Microporous and Mesoporous Materials*, **264**: 147-150.